

# Nonrelativistic spin splittings and altermagnetism in twisted bilayers of centrosymmetric antiferromagnets

Sajjan Sheoran\* and Saswata Bhattacharya†

Department of Physics, Indian Institute of Technology Delhi, New Delhi 110016, India

Magnetism-driven nonrelativistic spin splittings (NRSS) are promising for highly efficient spintronics applications. Although 2D centrosymmetric (in four-dimensional spacetime) antiferromagnets are abundant, they have not received extensive research attention owing to symmetry-forbidden spin polarization and magnetization. Here, we demonstrate a paradigm to harness NRSS by twisting the bilayer of centrosymmetric antiferromagnets with commensurate twist angles. We observe  $i$ -wave altermagnetism and spin-momentum locking by first-principles simulations and symmetry analysis on prototypical MnPSe<sub>3</sub> and MnSe antiferromagnets. The strength of NRSS (up to 80 meVÅ) induced by twisting is comparable to SOC-induced linear Rashba-Dresselhaus effects. The results also demonstrate how applying biaxial strain and a vertical electric field tune the NRSS. The findings reveal the untapped potential of centrosymmetric antiferromagnets and thus expand the material’s horizons in spintronics.

Spin splittings in the electronic structure of crystalline solids play a pivotal role in spintronics applications (e.g., spin transistor) [1, 2]. The conventional spin-orbit coupling (SOC) induced Rashba-Dresselhaus [3–6] in nonmagnetic and Zeeman effects in ferromagnetic (FM) materials create spin splittings under certain crystalline (i.e., inversion [ $\mathcal{P}$ ]) and time-reversal symmetry ( $\mathcal{T}$ ) breaking [7], respectively. SOC-induced spin splitting and resulting spin polarization engender spin-orbit torques [8], while FM spin polarization has been widely known for spin generation and detection [1]. However, the SOC effect introduces spin dephasing mechanisms [9–11], limiting the practical application. In addition, materials with heavy elements having significant SOC imparts additional challenges, including scarcity, toxicity, and instability. Therefore, nonrelativistic spin splitting (NRSS) is an important avenue to pursue.

Recently, antiferromagnetic (AFM) materials have emerged as viable substitutes for nonmagnetic and FM materials, benefiting from resilience towards stray fields, ultrafast dynamics, and magnetotransport effects [12–16]. The coupling of spin to lattice degrees of freedom via a staggered collinear compensated magnetism leads to alternating NRSS, termed altermagnetism [17–19]. Numerous efforts have been undertaken to investigate NRSS in AFM materials by breaking combined  $\mathcal{PT}\tau$  and/or  $U\tau$  symmetries, where  $U$  and  $\tau$  are spinor and translation symmetry, respectively [20–26]. Nevertheless, the majority of AFM spin splittings are limited to bulk materials (e.g., MnF<sub>2</sub> [21, 27], LaMnO<sub>3</sub>, and MnTiO<sub>3</sub> [23]), require SOC (e.g., MnS<sub>2</sub> [23] and ZnV<sub>2</sub>O<sub>4</sub> [28]), or external perturbation [29–31].

Since the experimental revelation of 2D magnetic ordering, 2D vdW magnetic materials have garnered significant attention in scientific research, emerging as promising contenders for future information technology. Inter-

estingly, two recent works focus on spin splitting in FM NiCl<sub>2</sub> [32] and FeBr<sub>2</sub> (although “hidden”) [33] monolayers vdW stacked antiferromagnetically. In contrast, antiferromagnetism-induced spin splitting among centrosymmetric materials with AFM order within each layer is not achieved due to  $\mathcal{PT}$  symmetry-enforced spin-degeneracy. Despite being abundant in nature, this impedes practical applications of 2D centrosymmetric AFM materials [34–38].

This study generates NRSS and altermagnetism in  $\mathcal{PT}$ -symmetric AFM monolayers vdW stacked with a relative twist. We perform density functional theory (DFT) simulations on twisted bilayer (tb-) MnPSe<sub>3</sub> and MnSe as prototypical candidates. The  $i$ -wave spin-momentum coupling arises in the 2D BZ for  $\theta$  ( $\neq 0^\circ, 60^\circ$ ) tb-MnPSe<sub>3</sub> and MnSe. Based on the symmetry analysis, we find that the strengths of NRSS along specific crystallographic  $k$ -paths are comparable to the conventional SOC-induced Rashba-Dresselhaus effects. Moreover, external perturbations (i.e., electric and strain fields) provide exceptional tunability to NRSS.

MnPSe<sub>3</sub> and MnSe (space group #162,  $P\bar{3}1m$ ) represent two distinct classes of vdW materials that possess exceptional exfoliation properties [34–38]. Unlike the majority of other 2D magnetic materials, they exhibit an AFM arrangement, conforming to the conventional collinear Néel order on the honeycomb lattice [Fig. 1]. This in-plane antiferromagnetism is different from the A-type antiferromagnetism observed in various other 2D vdW compounds, i.e., MnBi<sub>2</sub>Te<sub>4</sub> [39], CrI<sub>3</sub> [40], and CrSBr [41], where individual layers exhibit FM order but stack antiferromagnetically. The antiferromagnetism of MnPSe<sub>3</sub> is “truly” in-plane and differs from that of MnSe, where Mn ions with opposite magnetic moments (Mn<sub>A</sub> and Mn<sub>B</sub>) form unusual out-of-plane ordering within the individual layer. Note that the orientation of on-site magnetic moments concerning the lattice only matters if SOC is included. Therefore, nonrelativistic spin-group formalism is described as the symmetry transformation of decoupled real and spin space [18, 42–

\* phz198687@physics.iitd.ac.in

† saswata@physics.iitd.ac.in

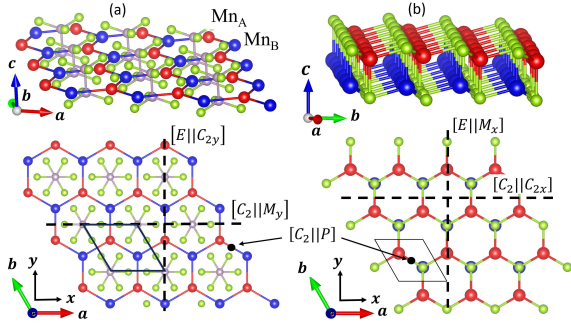


FIG. 1. Crystal structure of the monolayer (a)  $\text{MnPSe}_3$  and (b)  $\text{MnSe}$ . The red and blue spheres indicate Mn atoms with the opposite collinear magnetic densities. The brown and green spheres represent P and Se atoms, respectively. The Cartesian  $(x, y, z)$  coordinate system and the hexagonal unit cell (with solid black lines) are shown for each case. The nontrivial spin-group symmetries are also highlighted.  $E$  and  $C_2$  represent identity and two-fold rotation (about an axis perpendicular to spins) in spin-space, respectively.  $M_i$  and  $C_{2j}$  denote the mirror reflection perpendicular to the  $i$  axis and the two-fold rotation parallel to the  $j$  axis in real-space, respectively.  $\mathcal{P}$  represents the real-space inversion.

45]. The spin-symmetry operations  $[R_i||R_j]$  of monolayer  $\text{MnPSe}_3$  and  $\text{MnSe}$  are indicated in Fig. 1, where the transformation on the left (right) of the double vertical bar acts on the only spin (real) space. In addition, collinear magnets always have additional symmetry  $[\bar{C}_2||T]$  arising from spin-only groups, where  $\bar{C}_2$  is the two-fold rotation perpendicular to the collinear spin axis, followed by spin-space inversion.  $\text{Mn}_A$  and  $\text{Mn}_B$  sublattices are connected through  $[C_2||\mathcal{P}]$  symmetry in monolayer  $\text{MnPSe}_3$  and  $\text{MnSe}$ .  $[C_2||\mathcal{P}][\bar{C}_2||T] (\equiv \mathcal{PT}^1)$  symmetry transforms energy eigenstate  $E(k, \sigma)$  as  $[C_2||\mathcal{P}][\bar{C}_2||T]E(k, \sigma) = [C_2||\mathcal{P}]E(-k, \sigma) = E(k, -\sigma)$ , leading to spin degeneracy throughout the Brillouin zone (BZ). We have verified that through DFT+U calculations performed on the projector augmented wave method [46] based VASP [47] code (methods are detailed in Sect. I of supplemental material (SM) [48]). DFT simulated energy bands for monolayer  $\text{MnPSe}_3$  and  $\text{MnSe}$  are doubly degenerate (see Sect. II in SM [48]). The semiconducting  $\text{MnPSe}_3$  and  $\text{MnSe}$  have a magnetic moment of  $\sim 4.5\mu_B/\text{Mn}$  with weak interlayer coupling. In addition,  $[C_2||\tau]$  can also enforce spin-degeneracy by connecting opposite spin sublattices by translation ( $\tau$ ) as  $[C_2||\tau]E(k, \sigma) = E(k, -\sigma)$ . Since 2D systems have only in-plane components of momentum  $k_{||}$ , nonrelativistic Hamiltonian for 2D systems may have symmetries other than  $[C_2||\mathcal{P}]$  and  $[C_2||\tau]$  enforcing spin degeneracy. For example,  $[C_2||M_z]$  symmetry also enforces spin degeneracy throughout BZ in 2D materials, with  $M_z : M_z k_{||} = k_{||}$

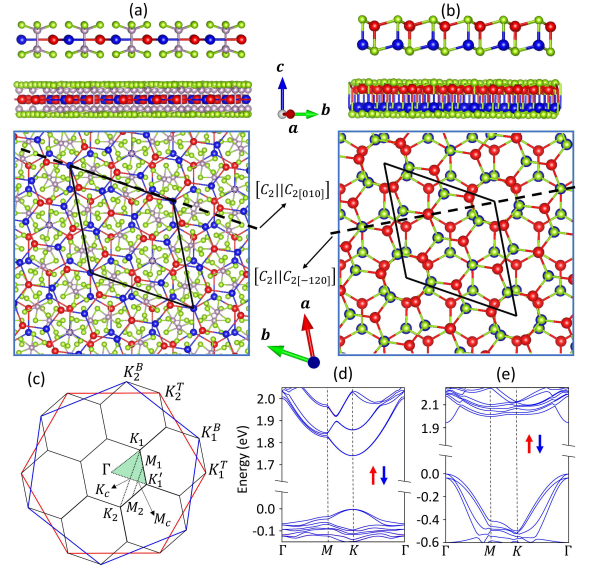


FIG. 2. The Moiré superlattices formed by twisting bilayer of (a)  $\text{MnPSe}_3$  and (b)  $\text{MnSe}$  by  $21.79^\circ$ . (c) The Moiré BZ construction uses BZs of the top and bottom layers. The large red and blue hexagons are the first BZ of the top and bottom layers, respectively, and black hexagons represent the BZ corresponding to the Moiré superlattice. Spin-polarized band structure of (d)  $\text{tb-MnPSe}_3$  and (e)  $\text{tb-MnSe}$  at the PBE level. The red and blue bands denote spin-up and spin-down states, respectively.

as a planer mirror reflection [see Sec. II of SM [48] for details]. That makes achieving NRSS even more difficult for 2D materials. In the case of  $\text{MnPSe}_3$  and  $\text{MnSe}$  monolayers,  $[C_2||M_z]$  is already broken [Figs. 1(a) and 1(b)], whereas type-III Shubnikov MSG ensures  $[C_2||\tau]$  symmetry-breaking [49]. The only symmetry preserving spin degeneracy is  $[C_2||\mathcal{P}]$  symmetry in monolayers  $\text{MnPSe}_3$  and  $\text{MnSe}$ .

Bilayer  $\text{MnSe}$  and  $\text{MnPSe}_3$  are obtained from monolayers with various high-symmetry stackings as used in Ref [30]. Spin-up and spin-down states are degenerate for AA, AA', AB, and BA stackings [see Sec. II of SM [48]]. The  $[C_2||\mathcal{P}]$  symmetry enforces double degeneracy in AA, AB, and BA, whereas double degeneracy in AA' stacking is protected by the  $[C_2||M_z]$ . Therefore, high-symmetry stackings are not an ideal for SOC-unrelated spin splitting in 2D  $\mathcal{PT}$ -symmetric antiferromagnets.

Commensurate twisted bilayers are obtained using coincidence lattice theory [50] by taking the AA bilayer as the untwisted limit to break  $\mathcal{PT}$  symmetry. A periodic lattice structure, including Moiré superlattice, can form with special twist angle  $\theta$ ,  $\cos \theta = \frac{n^2 + 4mn + m^2}{2(m^2 + mn + n^2)}$ , where  $m, n$  are whole numbers [51]. We only considered twist angles that resulted in reasonably sized commensurate supercells with the number of atoms in unit-cell fewer than 350. Figures 2(a) and 2(b) show relaxed crystal structures and Moiré patterns in  $\theta = 21.79^\circ$   $\text{tb-MnPSe}_3$  and  $\text{tb-MnSe}$  [see Moiré BZ in Fig. 2(c)]. Different pos-

<sup>1</sup> Therefore, we use “ $[C_2||\mathcal{P}]$ ” and “ $\mathcal{PT}$ ” interchangeably.

sible interlayer and intralayer magnetic couplings  $\uparrow\uparrow\uparrow$ ,  $\uparrow\downarrow\downarrow$ ,  $\uparrow\downarrow\uparrow$ , and  $\uparrow\uparrow\downarrow$  were considered to determine the preferred magnetic ordering [here, up and down arrows represent the relative magnetic moment direction on Mn atoms]. The most stable magnetic structure is  $\uparrow\downarrow\uparrow\downarrow$ , where magnetic order is intralayer and interlayer AFM [Figs. 2(a) and 2(b)]. Twist angle leads to small variation in the magnitude of local magnetic moments from 4.441 to 4.448  $\mu_B/\text{Mn}$  in tb-MnSe. The tb-MnPSe<sub>3</sub> and tb-MnSe are antiferromagnetic with opposite spin sublattices connected through the rotation symmetries ( $[\mathcal{C}_2|\mathcal{C}_{2[010]}]$  and  $[\mathcal{C}_2|\mathcal{C}_{2[-120]}]$ , respectively) with net zero magnetization [Figs. 2(a) and 2(b)]. In addition to Mn atoms, nonmagnetic ligands also contribute to  $\mathcal{PT}$  symmetry breaking in tb-MnPSe<sub>3</sub> and tb-MnSe.

Firstly, we compute the spin-polarized band structures of tb-MnPSe<sub>3</sub> and tb-MnSe along the high-symmetry paths (HSPs) [Figs. 2(d),(e)]. The bands are spin degenerate along HSPs due to special symmetries arising at arbitrary  $k$ -point on HSP. For instance,  $[\mathcal{C}_2|\mathcal{C}_{2[010]}]$  in tb-MnPSe<sub>3</sub> transforms spin-up to spin-down state along the  $\Gamma$ - $K$  path, enforcing degeneracy between them [see Sec. III of SM [48]]. However, this is not the case for any generic  $k$ -point. No symmetry transform spin-up to spin-down at generic  $k$ -point, leading to the lifting of Kramers degeneracy. Therefore, the full BZ analysis of spin splitting is required. We plot spin splitting energy  $\delta E [=E_{\uparrow}(k) - E_{\downarrow}(k)]$  of valence bands in tb-MnSe as a function of  $k$  [Fig. 3(a)]. The  $\delta E$  is invariant under real-space inversion [ $\delta E(k) = \delta E(-k)$ ] due to spin-only symmetry  $[\bar{\mathcal{C}}_2|T]$ , which transforms energy eigenstates  $[\bar{\mathcal{C}}_2|T]E(k, \sigma) = E(-k, \sigma)$ . Therefore, leading to 6-fold symmetric ( $[E|\mathcal{C}_6]$ ) planar  $i$ -wave spin-momentum coupling, which is different from the 3-fold symmetry of SOC-induced  $\delta E$  observed in well-known monolayer MoS<sub>2</sub> [52]. Similar patterns are also observed for  $\delta E$  of CB in tb-MnSe and VB in tb-MnPSe<sub>3</sub> (see Sect. III in SM). The maximum NRSS is observed at the orthocenter ( $H/H'$ ) of the triangle formed by  $\Gamma$ ,  $M$ , and  $K_1/K'_1$  points. Maximum splitting observed is 20.4, 4.2, and 5.1 meV for VB of tb-MnSe, CB of tb-MnSe, and VB of tb-MnPSe<sub>3</sub>, respectively. Maximum  $\delta E$  is smaller than well-known bulk antiferromagnets, i.e., MnF<sub>2</sub> [21], Fe<sub>2</sub>TeO<sub>6</sub> [31], and LaMnO<sub>3</sub> [23]. The  $\delta E$  observed in CB of tb-MnPSe<sub>3</sub> is negligible and beyond the accuracy of our calculations.

To understand the nature of NRSS, we plot band structures along both  $K_1$ - $K_c$ - $K_2$  and  $M_1$ - $M_c$ - $M_2$  directions [Figs. 3(b)-(e)]. Interestingly, linear NRSS is observed around  $K_c$  and  $M_c$  for VB and CB of tb-MnSe and VB of tb-MnPSe<sub>3</sub>. The spin splittings exhibit contrasting characteristics at the  $H$  and  $H'$  points, featuring distinct valleys and maximum strength, suggesting the potential for valleytronics applications in twisted bilayers of antiferromagnets [53, 54]. Note that the spin splittings around the  $\Gamma$  point, along the  $\Gamma$ - $H/H'$  direction, exhibit cubic characteristics, which result in their being relatively small and, as such, are excluded from the cur-

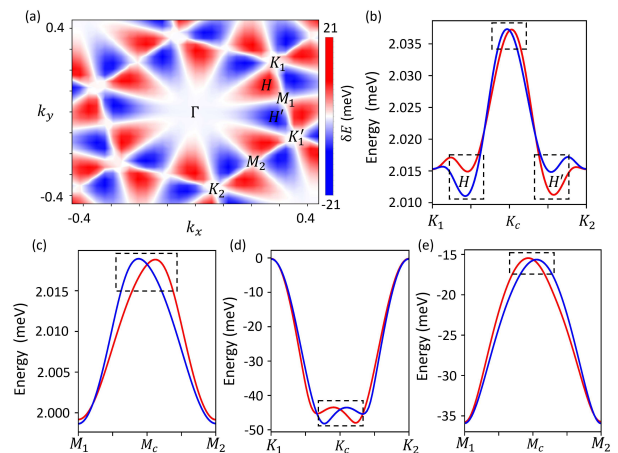


FIG. 3. (a) Spin splitting energy [ $\delta E = E_{\uparrow}(k) - E_{\downarrow}(k)$ ] distribution of valence band in 21.79° tb-MnSe. The units of  $k_x$  and  $k_y$  are  $\text{\AA}^{-1}$ . Conduction bands of tb-MnSe along the (b)  $K_1$ - $K_c$ - $K_2$  and (c)  $M_1$ - $M_c$ - $M_2$  paths [see Fig 2(c) for paths]. Valence bands of tb-MnPSe<sub>3</sub> along the (d)  $K_1$ - $K_c$ - $K_2$  and (e)  $M_1$ - $M_c$ - $M_2$  paths. The red and blue curves denote spin-up and spin-down bands, respectively. Black dashed squares represent prominent spin splittings. Fermi energy is set to valence band maximum.

rent discussion [55].

Spin splittings around  $M_c$  and  $K_c$  points are further analyzed using the symmetry-based model Hamiltonian, deduced using the “method of invariants” [55, 58]. The symmetry element (besides identity) of  $M_c/K_c$  point is  $[\mathcal{C}_2|\mathcal{C}_{2[010]}]$  and  $[\mathcal{C}_2|\mathcal{C}_{2[-120]}]$  for tb-MnPSe<sub>3</sub> and tb-MnSe, respectively [see Figs. 2(a) and 2(b)]. The symmetry invariant terms include  $\alpha q_y \sigma_z$  and  $q_y q_y^2 \sigma_z$  ( $i = x', y'$ ), where  $q = k - M_c/K_c$  are the momenta measured from  $M_c/K_c$  [see Sec. III of SM [48] for notation, derivation, and discussion]. Therefore, splitting is absent

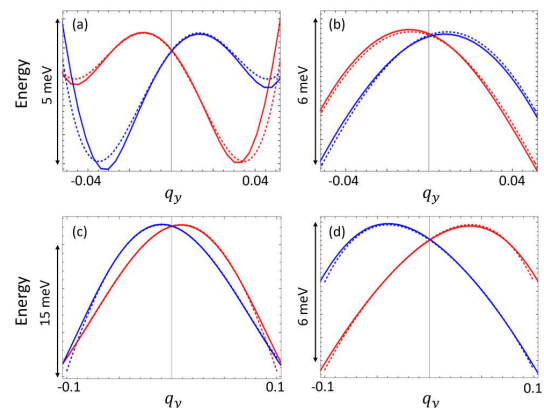


FIG. 4. Band structures of tb-MnPSe<sub>3</sub> around (a)  $K_c$  and (b)  $M_c$  along  $q_y$  direction. (c) and (d) are counterparts of (a) and (b), respectively, obtained for tb-MnSe. The solid and dotted lines are band structures obtained by DFT and the model described by Eq. 1, respectively.

TABLE I. Classification of 2D materials based on the MSG type, magnetic order and their impact on the NRSS. The relevant spin-group symmetry is also indicated in the case of spin-degeneracy at generic  $k$ .

Spin splitting prototype	Monolayer			Twisted bilayer	Examples
	Magnetic order	MSG type	NRSS at generic $k$	NRSS at generic $k$	
SST-1	Nonmagnetic	II	$\mathcal{X}([C_2  E])$	$\mathcal{X}([C_2  E])$	MoS <sub>2</sub> [56], PtSe <sub>2</sub> [57]
SST-2	Ferromagnetic	I/III	✓	✓	NiCl <sub>2</sub> , CrI <sub>3</sub> , CrN, CrSBr [32]
SST-3	Antiferromagnetic	III	$\mathcal{X}([C_2  \mathcal{P}]/[C_2  \mathcal{M}_z])$	✓	MnPSe <sub>3</sub> , MnSe [This work]
SST-4	Altermagnetic	I/III	✓	-	
SST-5	Antiferromagnetic	IV	$\mathcal{X}([C_2  \tau])$	-	

along the  $q_{x'}$  ( $K_c$ - $K'_1$  and  $M_c$ - $K'_1$ ) direction, whereas it is present along the  $q_{y'}$  direction ( $K_c$ - $K_{1/2}$  and  $M_c$ - $M_{1/2}$ ). To understand the NRSS along the  $q_{y'}$  direction, it is possible to write an effective Hamiltonian ( $H_{eff}$ ), up to third-order in  $k$ :

$$H_{eff} = \alpha q_{y'} \sigma_z + \eta q_{y'}^3 \sigma_z \quad (1)$$

$\alpha$  and  $\eta$  are the constants determining the strength of NRSS. The primary linear term in Eq. 1 leads to the linear splitting of spin-up and spin-down energy bands around  $M_c$  and  $K_c$  points, similar to the linearly split bands by SOC-induced Rashba and Dresselhaus effects. Note that spin splitting in Eq. 1 originates from altermagnetic ordering and is completely nonrelativistic. On the other hand, the Rashba-Dresselhaus effect is induced by the spin-orbit field originating from noncentrosymmetric sites and is of relativistic origin. We fit the energy levels around  $M_c$  and  $K_c$  along the  $q_{y'}$  direction to obtain spin-splitting parameters. The fits are obtained by minimization of the summation,  $S = \sum_{i=1}^2 \sum_q f(q) |\text{Det}[H_{eff}(q) - E^i(q)I]|^2$  over the  $i^{th}$  energy eigenvalues  $[E^i(q)]$  as training sets. We have also included a weight function  $f(q)$  with normal distribution to get a better fit near the spin-degenerate point and avoid overfitting. The obtained fits to the DFT energy levels of tb-MnPSe<sub>3</sub> and tb-MnSe are shown in Figs. 4(a)-4(d). The Hamiltonian in Eq 1 with  $\alpha=58.6$  meVÅ and  $\eta=34.2$  eVÅ<sup>3</sup> provide the best fit to the VBs of tb-MnPSe<sub>3</sub> around the  $K_c$  point [Fig. 4(a)]. Whereas  $\alpha=39.8$  meVÅ and  $\eta=3.5$  eVÅ<sup>3</sup> are observed for VBs of tb-MnPSe<sub>3</sub> around the  $M_c$  point, respectively [Fig. 4(b)]. Similarly, linear splitting strength of 35.4 and 60.7 meVÅ is observed in CBs of tb-MnSe around the  $K_c$  and  $M_c$  points, respectively [Figs. 4(c)-3(d)]. The NRSS is comparable to those experimentally reported in the literature (e.g., 10 meVÅ for KTaO<sub>3</sub> [59], 4.3 meVÅ for LaAlO<sub>3</sub>/SrTiO<sub>3</sub> interface [60], ~70 meVÅ in InGaAs/InAlAs interface [61], and 77 meVÅ for MoS<sub>2</sub> monolayer [62]). The growing field of twistronics makes NRSS observed in tb-MnPSe<sub>3</sub> and tb-MnSe experimentally accessible.

The 2D magnetic materials can be classified into five prototypes depending on the magnetic order, MSG, and whether NRSS is absent or present in a monolayer [Table I]. Spin degeneracy in nonmagnetic materials (SST-1) is enforced by  $[C_2||E]$  and remains preserved under twisting operations. In contrast, FM materials (SST-2) show NRSS in both monolayer limits and two layers

stacked antiferromagnetically with a twist [32]. Altermagnetic materials (SST-4) have opposite-spin sublattices connected through mirror-rotation symmetries with opposite-spin electronic states separated in the momentum space. MSG type-IV always has AFM order with  $[C_2||\tau]$  symmetry (SST-5) and necessitates SOC to induce spin splitting [23]. 2D AFM materials with MSG type-III containing  $[C_2||\mathcal{P}]$  ( $\mathcal{PT}$ ) or  $[C_2||\mathcal{M}_z]$  (SST-3) are unique, as NRSS is absent in the monolayer and presented in twisted bilayer. Therefore, the twisting operation generates splittings in SST-3 type materials, the most common magnetic ordering found in nature.

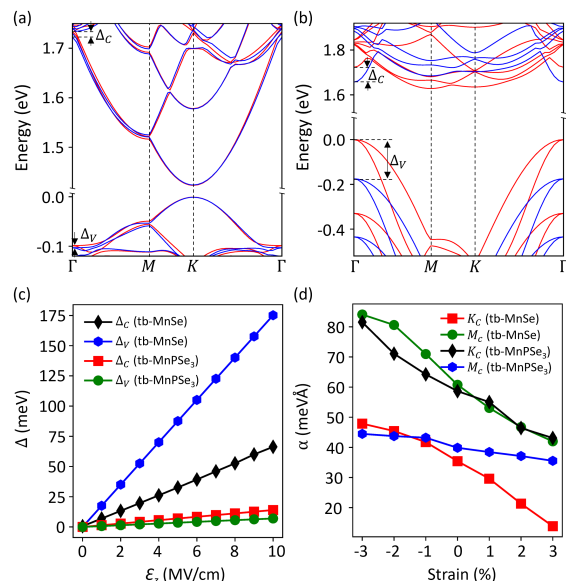


FIG. 5. Band structures of 21.79° (a) tb-MnPSe<sub>3</sub> and (b) tb-MnSe in the presence of the out-of-plane electric field ( $\mathcal{E}_z$ ) of strength 10 MV/cm. (c) The Zeeman spin splittings in the CB ( $\Delta_C$ ) and VB ( $\Delta_V$ ) of 21.79° tb-MnPSe<sub>3</sub> and tb-MnSe at  $\Gamma$  point as a function of  $\mathcal{E}_z$ . (d) The variation in  $\alpha$  (see Eq. 1) as a function of biaxial strain for 21.79° tb-MnPSe<sub>3</sub> and tb-MnSe.

Although controlling crystal symmetries in bulk materials is challenging, it has been shown that gating can effectively break the symmetries in 2D materials, including twisted bilayers [63–65]. In the following, we apply an out-of-plane electric field ( $\mathcal{E}_z$ ) to the tb-MnPSe<sub>3</sub> and tb-MnSe in DFT simulations self-consistently using the ap-

proach introduced by Neugebauer and Scheffler [66]. The electric field creates not only polarization but also magnetization by breaking opposite spin-sublattice transformation through the magnetoelectric coupling [67]. The Zeeman-like Hamiltonian under  $\mathcal{E}_z$  are given by [31],  $\hat{H}_Z = \lambda \mathcal{E}_z \sigma_z$ , where  $\lambda$  is coefficient determining coupling strength. In the presence of  $\mathcal{E}_Z$ , the spin degenerate levels at the high symmetry points ( $\Gamma$ ,  $M$ , and  $K$ ) and along HSPs will be split into two sublevels,  $E_+ = \lambda \mathcal{E}_z$  and  $E_- = -\lambda \mathcal{E}_z$  [Figs. 5(a)-5(c)]. We observe that the splitting induced by  $\mathcal{E}_z$  in tb-MnPSe<sub>3</sub> and tb-MnSe exhibits markedly distinct characteristics. Specifically, an electric field  $\mathcal{E}_z$  with a strength of 10 MV/cm results in nearly negligible splitting at the  $\Gamma$  point for tb-MnPSe<sub>3</sub>, suggesting a small  $\lambda$  [Figs. 5(a), 5(c)]. In contrast, for tb-MnSe, the  $\Gamma$  point experiences a significantly larger Zeeman-type splitting ( $\sim 175$ meV) induced by an electric field  $\mathcal{E}_z$  of 10 MV/cm [Figs. 5(b), 5(c)]. This disparity can be explained through structural analysis: in tb-MnPSe<sub>3</sub>, Mn atoms with opposite magnetic moments lie within the same  $z$ -plane, while in tb-MnSe, they are situated in different  $z$ -planes, thus supporting magnetoelectric coupling when an electric field is applied along the  $z$ -direction. On the contrary, when we compare the Zeeman splittings induced in the CB and VB of tb-MnSe at the  $\Gamma$  point [Fig. 5(b)], it becomes evident that the splitting in the VB is significantly greater in magnitude compared to that in the CB. This pronounced splitting in the VB of tb-MnSe can be attributed to the in-plane orbitals, which have wave functions segregated on different  $z$ -planes and, as a result, are more susceptible to the  $\mathcal{E}_z$ . In addition, tunability in electronic states can be achieved by the strain engineering of 2D materials [68]. The in-plane biaxial strain preserves the crystal symmetry, thus creating no additional splittings. However, the strength of NRSS ( $\alpha$ ) around  $K_c/M_c$  for twisted bilayers are modified under biaxial in-plane strain [Fig. 5(d)].  $\alpha$  increases with compressive strain and increases with tensile strain, providing exceptional tunability.

Similar effects were also investigated for other twist angles, including 9.43°, 13.17°, 27.79°, 32.20°, 38.21°, and 42.10° (see Sect. IV of SM [48]). The  $\delta E$  also depends upon the dispersiveness of energy bands, where  $\delta E$  increases with increasing band dispersion. The linear NRSS is more prominent for the twist angles around 30°, as the structure deviates from the  $\mathcal{PT}$ -symmetric ( $\theta = 0^\circ, 60^\circ$ ) counterparts by the highest amount. In addition, the strength of splitting is the same for twist angles  $\theta$  and  $60^\circ - \theta$  (see Sect. V of SM [48]). MnPSe<sub>3</sub>

and MnSe contain relatively lighter elements with negligible SOC effects (see Sect. VI of SM [48]). The Zeeman splitting observed in bilayer MnSe with a twist angle of  $\theta = 0^\circ$  is  $\sim 180$  meV under 10 MV/cm of the vertical electric field [30], nearly similar to 21.79° tb-MnSe of  $\sim 175$  meV with the same electric field. Similarly, the Zeeman effect in 0° tb-MnPSe<sub>3</sub> is negligible [29], like 21.79° tb-MnPSe<sub>3</sub>. Therefore, the order of Zeeman spin splitting depends much on how opposite spin-sublattices are arranged in the monolayer concerning the electric field and has less to do with the twist angle. Note that the models in this study include only spin degrees of freedom, thus revealing spin splitting qualitatively. For quantitative analysis, other degrees of freedom (i.e., orbital and sublattice) through first-principles or multiband tight-binding model calculations need to be included.

To summarize, we have shown that NRSS can be induced in 2D  $\mathcal{PT}$ -symmetric antiferromagnets by taking bilayers with a relative twist. By first-principles calculations and symmetry analysis, we further predict spin-moment coupling in 21.79° tb-MnPSe<sub>3</sub> and tb-MnSe that accommodate linear NRSS as large as  $\sim 90$  meVÅ. The lateral electric field split otherwise spin degenerate bands along the HSPs through magnetoelectric coupling, with more prominent effects in tb-MnSe. In addition, NRSSs are tunable using the biaxial strain. The measurement of these spin splittings can be conducted through well-established optical [29] and electrical transport [69] techniques commonly used in the field of spintronics. Employing antiferromagnets featuring spin-split bands as described in the present study may obviate the necessity for a heavy-metal layer, given that the current AFM mechanism yields a substantial magnitude of spin-moment splitting, even with lighter elements. Moreover, the low-Z antiferromagnets with even larger NRSSs can be predicted by the inverse design approach with desired functionality [70]. In addition, NRSS in Moiré-induced flat bands ( $\theta \lesssim 3^\circ$ ) can be an interesting avenue to prospect. We aspire to broaden the pool of available materials and enrich the field of AFM semiconductor spintronics [1, 2] through the complete realization of original devices.

*Acknowledgments.*—S.S. acknowledges CSIR, India, for the senior research fellowship [grant no. 09/086(1432)/2019-EMR-I]. S. B. acknowledges financial support from SERB under a core research grant (grant no. CRG/2019/000647) to set up High-Performance Computing (HPC) facility “Veena” at IIT Delhi for computational resources.

---

[1] I. Žutić, J. Fabian, and S. D. Sarma, Spintronics: Fundamentals and applications, *Reviews of modern physics* **76**, 323 (2004).  
 [2] A. Fert, Nobel lecture: Origin, development, and future of spintronics, *Reviews of modern physics* **80**, 1517 (2008).

[3] G. Dresselhaus, Spin-orbit coupling effects in zinc blende structures, *Physical Review* **100**, 580 (1955).  
 [4] E. Rashba, Properties of semiconductors with an extremum loop. i. cyclotron and combinational resonance in a magnetic field perpendicular to the plane of the loop, *Sov. Phys.-Solid State* **2**, 1109 (1960).

- [5] F. Vas'ko, Spin splitting in the spectrum of two-dimensional electrons due to the surface potential, *Soviet Journal of Experimental and Theoretical Physics Letters* **30**, 541 (1979).
- [6] Y. A. Bychkov and É. I. Rashba, Properties of a 2d electron gas with lifted spectral degeneracy, *JETP lett* **39**, 78 (1984).
- [7] A. F. Young, C. R. Dean, L. Wang, H. Ren, P. Cadden-Zimansky, K. Watanabe, T. Taniguchi, J. Hone, K. L. Shepard, and P. Kim, Spin and valley quantum hall ferromagnetism in graphene, *Nature Physics* **8**, 550 (2012).
- [8] C. Ciccarelli, L. Anderson, V. Tshitoyan, A. Ferguson, F. Gerhard, C. Gould, L. Molenkamp, J. Gayles, J. Železný, L. Šmejkal, *et al.*, Room-temperature spin-orbit torque in *ninmsb*, *Nature physics* **12**, 855 (2016).
- [9] R. J. Elliott, Theory of the effect of spin-orbit coupling on magnetic resonance in some semiconductors, *Physical Review* **96**, 266 (1954).
- [10] F. Seitz, D. Turnbull, and H. Ehrenreich, *Solid state physics* (Academic Press, 1968).
- [11] M. Dyakonov and V. Perel, Spin relaxation of conduction electrons in noncentrosymmetric semiconductors, *Soviet Physics Solid State, Ussr* **13**, 3023 (1972).
- [12] J. Han, R. Cheng, L. Liu, H. Ohno, and S. Fukami, Coherent antiferromagnetic spintronics, *Nature Materials* **22**, 684 (2023).
- [13] V. Baltz, A. Manchon, M. Tsoi, T. Moriyama, T. Ono, and Y. Tserkovnyak, Antiferromagnetic spintronics, *Reviews of Modern Physics* **90**, 015005 (2018).
- [14] T. Jungwirth, X. Marti, P. Wadley, and J. Wunderlich, Antiferromagnetic spintronics, *Nature nanotechnology* **11**, 231 (2016).
- [15] T. Jungwirth, J. Sinova, A. Manchon, X. Marti, J. Wunderlich, and C. Felser, The multiple directions of antiferromagnetic spintronics, *Nature Physics* **14**, 200 (2018).
- [16] J. Železný, P. Wadley, K. Olejník, A. Hoffmann, and H. Ohno, Spin transport and spin torque in antiferromagnetic devices, *Nature Physics* **14**, 220 (2018).
- [17] S. Pekar and E. Rashba, Combined resonance in crystals in inhomogeneous magnetic fields, *Zh. Eksperim. i Teor. Fiz.* **47** (1964).
- [18] L. Šmejkal, J. Sinova, and T. Jungwirth, Beyond conventional ferromagnetism and antiferromagnetism: A phase with nonrelativistic spin and crystal rotation symmetry, *Physical Review X* **12**, 031042 (2022).
- [19] L. Šmejkal, J. Sinova, and T. Jungwirth, Emerging research landscape of altermagnetism, *Physical Review X* **12**, 040501 (2022).
- [20] S. Hayami, Y. Yanagi, and H. Kusunose, Momentum-dependent spin splitting by collinear antiferromagnetic ordering, *Journal of the Physical Society of Japan* **88**, 123702 (2019).
- [21] L.-D. Yuan, Z. Wang, J.-W. Luo, E. I. Rashba, and A. Zunger, Giant momentum-dependent spin splitting in centrosymmetric low-*z* antiferromagnets, *Physical Review B* **102**, 014422 (2020).
- [22] S. Hayami, Y. Yanagi, and H. Kusunose, Bottom-up design of spin-split and reshaped electronic band structures in antiferromagnets without spin-orbit coupling: Procedure on the basis of augmented multipoles, *Physical Review B* **102**, 144441 (2020).
- [23] L.-D. Yuan, Z. Wang, J.-W. Luo, and A. Zunger, Prediction of low-*z* collinear and noncollinear antiferromagnetic compounds having momentum-dependent spin splitting even without spin-orbit coupling, *Physical Review Materials* **5**, 014409 (2021).
- [24] R. González-Hernández, L. Šmejkal, K. Vyborný, Y. Yahagi, J. Sinova, T. Jungwirth, and J. Železný, Efficient electrical spin splitter based on nonrelativistic collinear antiferromagnetism, *Physical Review Letters* **126**, 127701 (2021).
- [25] L. Šmejkal, A. B. Hellenes, R. González-Hernández, J. Sinova, and T. Jungwirth, Giant and tunneling magnetoresistance in unconventional collinear antiferromagnets with nonrelativistic spin-momentum coupling, *Physical Review X* **12**, 011028 (2022).
- [26] L.-D. Yuan and A. Zunger, Degeneracy removal of spin bands in collinear antiferromagnets with non-interconvertible spin-structure motif pair, *Advanced Materials*, 2211966 (2023).
- [27] P. Dufek, K. Schwarz, and P. Blaha, Electronic and magnetic structure of *mnf* 2 and *nif* 2, *Physical Review B* **48**, 12672 (1993).
- [28] T. Maitra and R. Valenti, Orbital order in *znv* 2 o 4, *Physical review letters* **99**, 126401 (2007).
- [29] N. Sivadas, S. Okamoto, and D. Xiao, Gate-controllable magneto-optic kerr effect in layered collinear antiferromagnets, *Physical Review Letters* **117**, 267203 (2016).
- [30] S. Sheoran and S. Bhattacharya, Multiple zeeman-type hidden spin splittings in *pt*-symmetric layered antiferromagnets, *Physical Review B* **109**, L020404 (2024).
- [31] H. J. Zhao, X. Liu, Y. Wang, Y. Yang, L. Bellaiche, and Y. Ma, Zeeman effect in centrosymmetric antiferromagnetic semiconductors controlled by an electric field, *Physical Review Letters* **129**, 187602 (2022).
- [32] R. He, D. Wang, N. Luo, J. Zeng, K.-Q. Chen, and L.-M. Tang, Nonrelativistic spin-momentum coupling in antiferromagnetic twisted bilayers, *Physical Review Letters* **130**, 046401 (2023).
- [33] L.-D. Yuan, X. Zhang, C. M. Acosta, and A. Zunger, Uncovering spin-orbit coupling-independent hidden spin polarization of energy bands in antiferromagnets, *Nature Communications* **14**, 5301 (2023).
- [34] R. Basnet, K. M. Kotur, M. Rybak, C. Stephenson, S. Bishop, C. Autieri, M. Birowska, and J. Hu, Controlling magnetic exchange and anisotropy by nonmagnetic ligand substitution in layered *m p x 3* ( $m = \text{ni, mn}$ ;  $x = \text{s, se}$ ), *Physical Review Research* **4**, 023256 (2022).
- [35] C. Autieri, G. Cuono, C. Noce, M. Rybak, K. M. Kotur, C. E. Agrapidis, K. Wohlfeld, and M. Birowska, Limited ferromagnetic interactions in monolayers of *mps3* ( $m = \text{mn and ni}$ ), *The Journal of Physical Chemistry C* **126**, 6791 (2022).
- [36] N. Pournaghavi, M. Islam, R. Islam, C. Autieri, T. Dietl, and C. M. Canali, Realization of the chern-insulator and axion-insulator phases in antiferromagnetic *mnte/bi* 2 (*se, te*) 3/*mnte* heterostructures, *Physical Review B* **103**, 195308 (2021).
- [37] M. Aapro, M. N. Huda, J. Karthikeyan, S. Kezilebieke, S. C. Ganguli, H. G. Herrero, X. Huang, P. Liljeroth, and H.-P. Komsa, Synthesis and properties of monolayer *mnse* with unusual atomic structure and antiferromagnetic ordering, *ACS nano* **15**, 13794 (2021).
- [38] S. Sattar, M. Islam, and C. Canali, Monolayer *mn x* and *janus x mn y* ( $x, y = \text{s, se, te}$ ): A family of two-dimensional antiferromagnetic semiconductors, *Physical Review B* **106**, 085410 (2022).

- [39] Y.-F. Zhao, L.-J. Zhou, F. Wang, G. Wang, T. Song, D. Ovchinnikov, H. Yi, R. Mei, K. Wang, M. H. Chan, *et al.*, Even-odd layer-dependent anomalous hall effect in topological magnet  $\text{mnbi}_2\text{te}_4$  thin films, *Nano letters* **21**, 7691 (2021).
- [40] N. Sivadas, S. Okamoto, X. Xu, C. J. Fennie, and D. Xiao, Stacking-dependent magnetism in bilayer  $\text{cr}_3$ , *Nano letters* **18**, 7658 (2018).
- [41] K. Lee, A. H. Dismukes, E. J. Telford, R. A. Wiscons, J. Wang, X. Xu, C. Nuckolls, C. R. Dean, X. Roy, and X. Zhu, Magnetic order and symmetry in the 2d semiconductor  $\text{crsbr}$ , *Nano Letters* **21**, 3511 (2021).
- [42] W. Brinkman and R. J. Elliott, Theory of spin-space groups, *Proceedings of the Royal Society of London. Series A. Mathematical and Physical Sciences* **294**, 343 (1966).
- [43] D. B. Litvin and W. Opechowski, Spin groups, *Physica* **76**, 538 (1974).
- [44] D. B. Litvin, Spin point groups, *Acta Crystallographica Section A: Crystal Physics, Diffraction, Theoretical and General Crystallography* **33**, 279 (1977).
- [45] P. Liu, J. Li, J. Han, X. Wan, and Q. Liu, Spin-group symmetry in magnetic materials with negligible spin-orbit coupling, *Physical Review X* **12**, 021016 (2022).
- [46] G. Kresse and D. Joubert, From ultrasoft pseudopotentials to the projector augmented-wave method, *Physical review b* **59**, 1758 (1999).
- [47] G. Kresse and J. Furthmüller, Efficient iterative schemes for ab initio total-energy calculations using a plane-wave basis set, *Physical review B* **54**, 11169 (1996).
- [48] See Supplemental Material at [link to be inserted by publisher] for computational methods, symmetry analysis of monolayer, bilayer, and twisted bilayers, results for twist angles other than  $21.79^\circ$ , correlation between twist angle  $\theta$  and  $60^\circ - \theta$ , and effect of spin-orbit coupling. The Supplemental Material also includes Refs. [18, 21, 29, 30, 46, 47, 49, 51, 56, 66, 71–89].
- [49] M. S. Dresselhaus, G. Dresselhaus, and A. Jorio, *Group theory: application to the physics of condensed matter* (Springer Science & Business Media, 2007).
- [50] K. Uchida, S. Furuya, J.-I. Iwata, and A. Oshiyama, Atomic corrugation and electron localization due to moiré patterns in twisted bilayer graphenes, *Phys. Rev. B* **90**, 155451 (2014).
- [51] J. L. Dos Santos, N. Peres, and A. C. Neto, Graphene bilayer with a twist: Electronic structure, *Physical review letters* **99**, 256802 (2007).
- [52] H. Jafari, E. Barts, P. Przybysz, K. Tenzin, P. J. Kowalczyk, P. Dabrowski, and J. Sławińska, Robust zeeman-type band splitting in sliding ferroelectrics, *arXiv:2308.15241* (2023).
- [53] S. Sheoran, M. Jain, R. Moulik, and S. Bhattacharya, Probing the uniaxial strain-dependent valley drift and berry curvature in monolayer  $\text{mosi}_2\text{n}_4$ , *Physical Review Materials* **7**, 114003 (2023).
- [54] S. Sheoran, A. Phutela, R. Moulik, and S. Bhattacharya, Manipulation of valley and spin properties in two-dimensional janus  $\text{wsigez}_4$  ( $z = \text{n, p, as}$ ) through symmetry control, *The Journal of Physical Chemistry C* **127**, 11396 (2023).
- [55] H. J. Zhao, H. Nakamura, R. Arras, C. Paillard, P. Chen, J. Gosteau, X. Li, Y. Yang, and L. Bellaiche, Purely cubic spin splittings with persistent spin textures, *Physical Review Letters* **125**, 216405 (2020).
- [56] M. H. Naik and M. Jain, Ultraflatbands and shear solitons in moiré patterns of twisted bilayer transition metal dichalcogenides, *Physical review letters* **121**, 266401 (2018).
- [57] L. Xu, H. Liu, C. Song, X. Li, F. Li, D. Li, L. Wang, X. Bai, and J. Qi, Evolution of interlayer stacking orders and rotations in bilayer  $\text{ptse}_2$  visualized by stem, *2D Materials* **8**, 025014 (2021).
- [58] L. Tao and E. Y. Tsymlal, Persistent spin texture enforced by symmetry, *Nature communications* **9**, 2763 (2018).
- [59] S. Varotto, A. Johansson, B. Göbel, L. M. Vicente-Arche, S. Mallik, J. Bréhin, R. Salazar, F. Bertran, P. L. Fèvre, N. Bergeal, *et al.*, Direct visualization of rashba-split bands and spin/orbital-charge interconversion at  $\text{ktao}_3$  interfaces, *Nature Communications* **13**, 6165 (2022).
- [60] G. J. Omar, W. Kong, H. Jani, M. Li, J. Zhou, Z. S. Lim, S. Prakash, S. Zeng, S. Hooda, T. Venkatesan, *et al.*, Experimental evidence of  $t_2g$  electron-gas rashba interaction induced by asymmetric orbital hybridization, *Physical Review Letters* **129**, 187203 (2022).
- [61] J. Nitta, T. Akazaki, H. Takayanagi, and T. Enoki, Gate control of spin-orbit interaction in an inverted  $\text{in}_0.53\text{ga}_{0.47}\text{as}/\text{in}_{0.52}\text{al}_{0.48}$  heterostructure, *Physical Review Letters* **78**, 1335 (1997).
- [62] T. Hu, F. Jia, G. Zhao, J. Wu, A. Stroppa, and W. Ren, Intrinsic and anisotropic rashba spin splitting in janus transition-metal dichalcogenide monolayers, *Physical Review B* **97**, 235404 (2018).
- [63] A. Weston, E. G. Castanon, V. Enaldiev, F. Ferreira, S. Bhattacharjee, S. Xu, H. Corte-León, Z. Wu, N. Clark, A. Summerfield, *et al.*, Interfacial ferroelectricity in marginally twisted 2d semiconductors, *Nature nanotechnology* **17**, 390 (2022).
- [64] S. Talkington and E. J. Mele, Electric-field-tunable band gap in commensurate twisted bilayer graphene, *Physical Review B* **107**, L041408 (2023).
- [65] S. Sheoran, S. Monga, A. Phutela, and S. Bhattacharya, Coupled spin-valley, rashba effect, and hidden spin polarization in  $\text{wsi}_2\text{n}_4$  family, *The Journal of Physical Chemistry Letters* **14**, 1494 (2023).
- [66] J. Neugebauer and M. Scheffler, Adsorbate-substrate and adsorbate-adsorbate interactions of na and k adlayers on al (111), *Physical Review B* **46**, 16067 (1992).
- [67] M. Fiebig, Revival of the magnetoelectric effect, *Journal of physics D: applied physics* **38**, R123 (2005).
- [68] Z. Dai, L. Liu, and Z. Zhang, Strain engineering of 2d materials: issues and opportunities at the interface, *Advanced Materials* **31**, 1805417 (2019).
- [69] D.-F. Shao, Y.-Y. Jiang, J. Ding, S.-H. Zhang, Z.-A. Wang, R.-C. Xiao, G. Gurung, W. Lu, Y. Sun, and E. Y. Tsymlal, Néel spin currents in antiferromagnets, *Physical Review Letters* **130**, 216702 (2023).
- [70] A. Zunger, Inverse design in search of materials with target functionalities, *Nature Reviews Chemistry* **2**, 0121 (2018).
- [71] J. P. Perdew, K. Burke, and M. Ernzerhof, Generalized gradient approximation made simple, *Physical review letters* **77**, 3865 (1996).
- [72] S. Grimme, Semiempirical gga-type density functional constructed with a long-range dispersion correction, *Journal of computational chemistry* **27**, 1787 (2006).
- [73] A. Liechtenstein, V. I. Anisimov, and J. Zaanen, Density-functional theory and strong interactions: Orbital order-

- ing in mott-hubbard insulators, *Physical Review B* **52**, R5467 (1995).
- [74] M. I. Aroyo, J. M. Perez-Mato, C. Capillas, E. Kroumova, S. Ivantchev, G. Madariaga, A. Kirov, and H. Wondratschek, Bilbao crystallographic server: I. databases and crystallographic computing programs, *Zeitschrift für Kristallographie-Crystalline Materials* **221**, 15 (2006).
- [75] L. Elcoro, B. Bradlyn, Z. Wang, M. G. Vergniory, J. Cano, C. Felser, B. A. Bernevig, D. Orobengoa, G. Flor, and M. I. Aroyo, Double crystallographic groups and their representations on the bilbao crystallographic server, *Journal of Applied Crystallography* **50**, 1457 (2017).
- [76] H. T. Stokes and D. M. Hatch, Findsym: program for identifying the space-group symmetry of a crystal, *Journal of Applied Crystallography* **38**, 237 (2005).
- [77] Y. Hinuma, G. Pizzi, Y. Kumagai, F. Oba, and I. Tanaka, Band structure diagram paths based on crystallography, *Computational Materials Science* **128**, 140 (2017).
- [78] V. Wang, N. Xu, J.-C. Liu, G. Tang, and W.-T. Geng, Vaspkit: A user-friendly interface facilitating high-throughput computing and analysis using vasp code, *Computer Physics Communications* **267**, 108033 (2021).
- [79] U. Herath, P. Tavazde, X. He, E. Bousquet, S. Singh, F. Muñoz, and A. H. Romero, Pyprocar: A python library for electronic structure pre/post-processing, *Computer Physics Communications* **251**, 107080 (2020).
- [80] A. Jain, S. P. Ong, G. Hautier, W. Chen, W. D. Richards, S. Dacek, S. Cholia, D. Gunter, D. Skinner, G. Ceder, *et al.*, Commentary: The materials project: A materials genome approach to accelerating materials innovation, *APL materials* **1** (2013).
- [81] S. V. Gallego, J. M. Perez-Mato, L. Elcoro, E. S. Tasci, R. M. Hanson, K. Momma, M. I. Aroyo, and G. Madariaga, Magdata: towards a database of magnetic structures. i. the commensurate case, *Journal of Applied Crystallography* **49**, 1750 (2016).
- [82] W. R. Inc., *Mathematica, Version 13.3*, champaign, IL, 2023.
- [83] X. Liu, A. P. Pyatakov, and W. Ren, Magnetoelectric coupling in multiferroic bilayer vs 2, *Physical Review Letters* **125**, 247601 (2020).
- [84] G. Constantinescu, A. Kuc, and T. Heine, Stacking in bulk and bilayer hexagonal boron nitride, *Physical review letters* **111**, 036104 (2013).
- [85] L. Tao and E. Y. Tsymlal, Perspectives of spin-textured ferroelectrics, *Journal of Physics D: Applied Physics* **54**, 113001 (2021).
- [86] S. Calder, A. Haglund, A. I. Kolesnikov, and D. Mandrus, Magnetic exchange interactions in the van der waals layered antiferromagnet mn p se 3, *Physical Review B* **103**, 024414 (2021).
- [87] M. Milivojević, M. Orozović, S. Picozzi, M. Gmitra, and S. Stavrić, Interplay of altermagnetism and weak ferromagnetism in two-dimensional ruf  $\alpha_4$ , arXiv preprint arXiv:2401.15424 (2024).
- [88] T. Adamantopoulos, M. Merte, F. Freimuth, D. Go, M. Ležaić, W. Feng, Y. Yao, J. Sinova, L. Šmejkal, S. Blügel, *et al.*, Spin and orbital magnetism by light in rutile altermagnets, arXiv preprint arXiv:2403.10235 (2024).
- [89] S. Bhowal and N. A. Spaldin, Ferroically ordered magnetic octupoles in d-wave altermagnets, *Physical Review X* **14**, 011019 (2024).